Syntheses and Redox Properties of Bis(hydroxoruthenium) Complexes with Quinone and Bipyridine Ligands. Water-Oxidation Catalysis

Tohru Wada, Kiyoshi Tsuge, and Koji Tanaka*

Institute for Molecular Science and Department of Structural Molecular Science, Graduate University for Advanced Studies, 38 Nishigonaka, Myodaiji, Okazaki, Aichi, 444-8585 Japan

Received May 23, 2000

The novel bridging ligand 1,8-bis(2,2′:6′,2″-terpyridyl)anthracene (btpyan) is synthesized by three reactions from 1,8-diformylanthracene to connect two $[Ru(L)(OH)]^+$ units (L = 3,6-di-*tert*-butyl-1,2-benzoquinone (3,6-^{t}Bu$_2$-qui) and 2,2′-bipyridine (bpy)). An addition of ^{t}BuOK (2.0 equiv) to a methanolic solution of $[Ru^{II}_2(OH)_2$(3,6-^{t}Bu$_2$qui)$_2$(btpyan)](SbF$_6$)$_2$ ([**1**](SbF$_6$)$_2$) results in the generation of $[Ru^{II}_2(O)_2$(3,6-^{t}Bu$_2$sq)$_2$(btpyan)]^0 (3,6-^{t}Bu$_2$sq = 3,6-di-*tert*-butyl-1,2-semiquinone) due to the reduction of quinone coupled with the dissociation of the hydroxo protons. The resultant complex $[Ru^{II}_2(O)_2$(3,6-^{t}Bu$_2$sq)$_2$(btpyan)]^0 undergoes ligand-localized oxidation at $E_{1/2}$ = +0.40 V (vs Ag/AgCl) to give $[Ru^{II}_2(O)_2$(3,6-^{t}Bu$_2$qui)$_2$(btpyan)]$^{2+}$ in MeOH solution. Furthermore, metal-localized oxidation of $[Ru^{II}_2(O)_2$(3,6-^{t}Bu$_2$qui)$_2$(btpyan)]$^{2+}$ at E_p = +1.2 V in CF_3CH_2OH/ether or water gives $[Ru^{III}_2(O)_2$(3,6-^{t}Bu$_2$qui)$_2$(btpyan)]$^{4+}$, which catalyzes water oxidation. Controlled-potential electrolysis of [**1**](SbF$_6$)$_2$ at +1.70 V in the presence of H_2O in CF_3CH_2OH evolves dioxygen with a current efficiency of 91% (21 turnovers). The turnover number of O_2 evolution increases to 33 500 when the electrolysis is conducted in water (pH 4.0) by using a [**1**](SbF$_6$)$_2$-modified ITO electrode. On the other hand, the analogous complex $[Ru^{II}_2(OH)_2(bpy)_2$(btpyan)](SbF$_6$)$_2$ ([**2**](SbF$_6$)$_2$) shows neither dissociation of the hydroxo protons, even in the presence of a large excess of ^{t}BuOK, nor activity for the oxidation of H_2O under similar conditions.

Introduction

Oxidation of water by the four-electron process shown in eq 1 is thermodynamically more favorable than that via a pathway

$$2H_2O \rightarrow O_2 + 4H^+ + 4e^- \quad (1)$$

involving sequential mono- or dielectron processes.[1] Molecular catalysts aimed at water oxidation to O_2 are required to have two or four metals at least, since a metal atom usually operates as the redox center of the one- or two-electron-transfer process. In photosystem II, the O_2-evolving center (OEC) is composed of a tetranuclear Mn cluster with two bis(μ-oxo) dimeric Mn units[2] and several mechanisms for O_2 evolution through high-valent Mn═O or Mn−O−Mn species are proposed.[2−4] A variety of metal complexes have been prepared as structural models for the OEC, and four-electron oxidation of water has been attained with only a few dinuclear metal (Mn, Ru) complexes.[5,6] We have briefly reported a water oxidation catalyzed by the dinuclear quinone complex [**1**](SbF$_6$)$_2$ in water.[7]

This paper reports in detail the redox behavior of $[\mathbf{1}]^{2+}$ coupled with the acid−base equilibrium of the hydroxo groups and elucidates the role of quinone $[\mathbf{1}]^{2+}$ in the oxidation of water by the comparison of the catalytic activity between of $[\mathbf{1}]^{2+}$ and the analogous 2,2′-bipyridine complex [**2**](SbF$_6$)$_2$ (see Chart 1 for structures).

Experimental Section

Materials. 1,8-Bis(hydroxymethyl)anthracene, 2-acetylpyridine, and triflic acid were purchased from Tokyo Kasei Organic Chemicals. $RuCl_3$ was purchased from Furuya Metal Co., Ltd., $NaSbF_6$ from Aldrich Chemical Co., Inc., and dehydrated pyridine from Wako Pure Chemical Industries, Ltd. CH_2Cl_2 was dried and distilled over calcium dichloride, and other solvents were distilled just prior to use.

Preparations. 1,8-Diformylanthracene. 1,8-Bis(hydroxymethyl)-anthracene (2.0 g, 8.4 mmol) and pyridinium chlorochromate (3.6 g, 17 mmol) were mixed with silica gel 60 (200 mesh, 3.6 g) in a 500 mL flask, and CH_2Cl_2 (200 mL) was then added. The reaction mixture was stirred for 3 h at room temperature, during which the suspension became dark brown. The mixture was eluted with a short Florisil column, and the eluate was evaporated to dryness to give a yellow solid. Crystallization of the crude product in benzene gave yellow-green crystals. Yield: 1.6 g (82%). Anal. Calcd for $C_{16}H_{10}O_2$: C, 82.04; H, 4.30. Found: C, 81.74; H, 4.65. ^{1}H NMR (CD_2Cl_2): δ 7.80 (dd, *J*

* To whom correspondence should be addressed at the Institute for Molecular Science.

(1) (a) Lehn, J.-M.; Sauvage, J.-P.; Ziessel, R. *N. J. Chim.* **1979**, *3*, 423. (b) Rüttinger, W.; Dismukes, G. C. *Chem. Rev.* **1997**, *97*, 1.
(2) (a) Yachandra, V. K.; DeRose, V. J.; Latimer, M. J.; Mukerji, I.; Sauer, K.; Klein, M. P. *Science* **1993**, *260*, 675. (b) Yachandra, V. K.; Sauer, K.; Klein, M. P. *Chem. Rev.* **1996**, *96*, 2927.
(3) (a) Wieghardt, K. *Angew. Chem., Int. Ed. Engl.* **1994**, *33*, 725. (b) Manchanda, R.; Brudvig, G. W.; Crabtree, R. H. *Coord. Chem. Rev.* **1995**, *144*, 1. (c) Hoganson, C. W.; Babcock, G. T. *Science* **1997**, *227*, 1953. (d) Rüttinger, W.; Dismukes, G. C. *Chem. Rev.* **1997**, *97*, 1. (e) Limburg, J.; Szalai, V. A.; Brudvig, G. W. *J. Chem. Soc., Dalton Trans.* **1999**, 1353. (f) Cua, A.; Stewart, D. H.; Reifler, M. J.; Brudvig, G. W.; Bocian, D. F. *J. Am. Chem. Soc.* **2000**, *122*, 2069.
(4) Limburg, J.; Vrettos, J. S.; Liable-Sands, L. M.; Reingold, A. L.; Crabtree, R. H.; Brudvig, G. W. *Science* **1999**, *283*, 1524.
(5) Natuta, Y.; Sasyama, M.; Sasaki, T. *Angew. Chem.* **1994**, *106*, 1964; *Angew. Chem., Int. Ed. Engl.* **1994**, *33*, 1939.
(6) (a) Gersten, S. W.; Samuels, G. J.; Meyer, T. J. *J. Am. Chem. Soc.* **1982**, *104*, 4029. (b) Gilbert, J. A.; Eggleston, D. S.; Murphy, W. R., Jr.; Gselowitz, D. A.; Gersten, S. W.; Hodgson, D. J.; Meyer, T. J. *J. Am. Chem. Soc.* **1985**, *107*, 3855. (c) Rotzinger, F. P.; Munalli, S.; Comte, P. J.; Hurst, K.; Gratzel, M.; Pern, F.-J.; Frank, A. J. *J. Am. Chem. Soc.* **1987**, *109*, 6619. (d) Chronister, C. W.; Binstead, R. A.; Ni, J.; Meyer, T. J. *Inorg. Chem.* **1997**, *36*, 3814.
(7) Wada, T.; Tsuge, K.; Tanaka, K. *Angew. Chem.* **2000**, *112*, 1542; *Angew. Chem., Int. Ed. Engl.* **2000**, *39*, 1479.

10.1021/ic000552i CCC: $20.00
Published on Web 12/12/2000

Chart 1

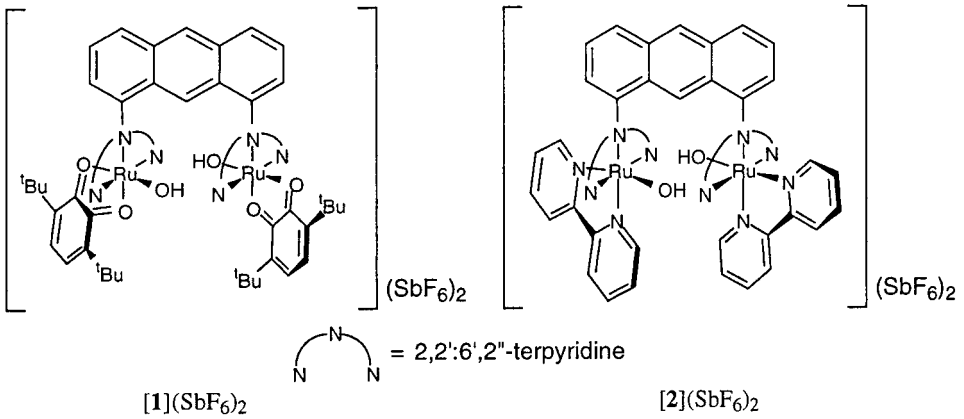

[**1**](SbF$_6$)$_2$ [**2**](SbF$_6$)$_2$

= 8.3, 6.8 Hz, 2 H, C*H*$_{anthracene}$), 8.20 (dd, J = 6.8, 1.0 Hz, 2 H, C*H*$_{anthracene}$), 8.41 (d, J = 8.5 Hz, 2 H, C*H*$_{anthracene}$), 8.70 (s, 1 H, C*H*$_{anthracene}$), 10.60 (s, 2 H, C*H*$_{anthracene}$), 11.23 (s, 2 H, C*H*$_{formyl}$). MS (EI): m/z 234 (M^+).

1,8-Bis[3-(2-pyridyl)-3-oxo-1-propenyl]anthracene (A). 2-Acetylpyridine (1.7 g, 14 mmol) was added to a stirred ethanol/H_2O solution (100 mL, 50/50 v/v) containing 1,8-diformylanthracene (1.6 g, 6.9 mmol) and NaOH (0.56 g, 14 mmol) in a 200 mL flask. Then, the reaction mixture was further stirred at room temperature for 3 h, during which a yellow powder precipitated out of the solution. The product was filtered off and crystallized from benzene as yellow crystals. Yield: 3.0 g (96%). Anal. Calcd for $C_{30}H_{20}N_2O_2$: C, 81.80; H, 4.58; N, 6.36. Found: C, 81.63; H, 4.60; N, 6.91. ^{1}H NMR (CD_2Cl_2): δ 7.51 (dd, J = 7.5, 4.6 Hz, 2 H, C*H*$_{pyridyl}$), 7.56 (dd, J = 8.5, 7.1 Hz, 2 H, C*H*$_{anthracene}$), 7.91 (dd, J = 7.8, 7.5 Hz, 2 H, C*H*$_{pyridyl}$), 8.06 (d, J = 7.1 Hz, 2 H, C*H*$_{anthracene}$), 8.11 (d, J = 8.5, 7.1 Hz, 2 H, C*H*$_{anthracene}$), 8.25 (d, J = 7.8 Hz, 2 H, C*H*$_{pyridyl}$), 8.41 (d, J = 15.6 Hz, 2 H, =C*H*$_{vinyl}$), 8.53 (s, 1 H, C*H*$_{anthracene}$), 8.81 (d, J = 4.6 Hz, 2 H, C*H*$_{pyridyl}$), 9.02 (d, J = 15.6 Hz, 2 H, =C*H*$_{vinyl}$), 9.30 (s, 1 H, C*H*$_{anthracene}$). MS (EI): m/z 440 (M^+).

1,8-Bis(2,2′:6′,2″-terpyridyl)anthracene (BTPYAN). 1,8-Bis(enonyl)anthracene **A** (500 mg, 1.1 mmol) and ^{t}BuOK (62 mg, 0.55 mmol, 25 mol % based on the amount of 2-acetylpyridine used) were dissolved in dry pyridine (50 mL) in a 100 mL flask, and the solution was stirred under N_2. 2-Acetylpyridine (266 mg, 2.2 mmol) was added, and the resultant solution was heated at 50 °C for 8 h. Solvent was evaporated in vacuo to dryness to give a reddish brown solid mainly composed of 1,8-bis[1,5-bis(2-pyridyl)-1,5-dioxo-3-pentyl]anthracene (**B**). This mixture was used as it was in the following reactions because of difficulties in achieving complete purification of **B**. Crude 1,8-bis(dionyl)anthracene **B** was dissolved in ethanol (50 mL) containing $AcONH_4$ (500 mg, large excess), and the solution was refluxed for 3 h in the air. The pale yellow powder that appeared in the solution was isolated by filtration and purified by HPLC (Japan Analytical Industry Co., Ltd., LC-908) with a GPC column using $CHCl_3$ as the eluent. Yield: 281 mg (40%). BTPYAN gradually decomposed upon exposure to room light. Anal. Calcd for $C_{44}H_{28}N_6$: C, 82.48; H, 4.40; N, 13.12. Found: C, 82.50; H, 4.63; N, 13.04. ^{1}H NMR ($CDCl_3$): δ 7.12 (dd, J = 7.3, 5.4 Hz, 4 H, C*H*$_{pyridyl}$), 7.58 (m, 4 H, C*H*$_{anthracene}$), 7.74 (dd, J = 7.8, 7.3 Hz, 4 H, C*H*$_{pyridyl}$), 8.11 (d, J = 8.3 Hz, 4 H, C*H*$_{anthracene}$), 8.29 (d, J = 7.8 Hz, 4 H, C*H*$_{pyridyl}$), 8.39 (d, J = 4.8 Hz, 4 H, C*H*$_{pyridyl}$), 8.49 (s, 4 H, C*H*$_{pyridyl}$), 8.59 (s, 1 H, C*H*$_{anthracene}$), 8.94 (s, 1 H, C*H*$_{anthracene}$). MS (FAB): m/z 641 (MH^+).

[Ru$_2$Cl$_6$(btpyan)]·5H$_2$O. An MeOH solution (30 mL) of $RuCl_3$ (128 mg, 0.62 mmol) and BTPYAN (200 mg, 0.31 mmol) was deoxygenated with a stream of nitrogen gas for 30 min, after which the solution was heated at reflux for 3 h under N_2. The dark brown solid that precipitated was filtered off and washed with MeOH (5 mL, three times) and acetone (5 mL, three times) to remove unreacted $RuCl_3$ and BTPYAN. Yield: 222 mg (68%). Anal. Calcd for $C_{44}H_{28}N_6Cl_6Ru_2$·$5H_2O$: C, 46.13; H, 3.34; N, 7.34. Found: C, 45.85; H, 2.95; N, 7.08.

[Ru$_2$(OAc)(3,6-^{t}Bu$_2$sq)$_2$(btpyan)](SbF$_6$)·4H$_2$O. A deoxygenated MeOH solution of AcOK (373 mg, 3.8 mmol) was added by syringe to an MeOH suspension (30 mL) of [Ru_2Cl_6(btpyan)]·$5H_2O$ (200 mg, 0.19 mmol) and 3,6-di-*tert*-butyl-1,2-catechol (84 mg, 0.38 mmol) under N_2. The reaction mixture was stirred for 4 days at room temperature under N_2. Insoluble [Ru_2Cl_6(btpyan)] gradually dissolved into MeOH, and the solution became purple. After the solution was concentrated to ca. 5 mL under reduced pressure, 15 mL of acetone was added and excess AcOK was filtered off. [Ru_2(OAc)(3,6-^{t}Bu$_2$sq)$_2$(btpyan)](AcO) was purified by column chromatography using Alumina A-super I (ICN Biomedicals GmbH) and acetone/EtOH as the eluent. An aqueous solution of $NaSbF_6$ was added to the purple fraction, and evaporation of acetone from the mixture gave a purple powder. Yield: 175 mg (56%). Anal. Calcd for $C_{74}H_{71}O_6N_6F_6Ru_2Sb$·$4H_2O$: C, 53.86; H, 4.82; N, 5.09. Found: C, 53.95; H, 4.42; N, 4.74. ESI-MS: m/z 1343 ([Ru_2(OAc)(3,6-^{t}Bu$_2$sq)$_2$(btpyan)]$^+$). Electronic absorption data (MeOH solution): λ_{max} 845 nm (ϵ 6120 M^{-1} cm^{-1}).

[Ru$_2$(OH)(3,6-^{t}Bu$_2$qui)$_2$(btpyan)](SbF$_6$)$_2$. CF_3SO_3H (200 mL) was added to an MeOH solution (30 mL) of [Ru_2(OAc)(3,6-^{t}Bu$_2$sq)$_2$(btpyan)](SbF$_6$)·$4H_2O$ (100 mg, 0.061 mmol). The resulting purple solution was stirred for 1 day, and its color became violet. This solution was evaporated to ca. 10 mL, followed by the addition of $NaSbF_6$, giving a violet powder. Yield: 175 mg (76%). Anal. Calcd for $C_{72}H_{70}O_6N_6F_{12}Ru_2Sb_2$: C, 48.34; H, 3.94; N, 4.70. Found: C, 48.39; H, 3.85; N, 4.64. ESI-MS: m/z 659 ([Ru_2(OH)$_2$(3,6-^{t}Bu$_2$qui)$_2$(btpyan)]$^{2+}$). Electronic absorption data (MeOH solution): λ_{max} 576 nm (ϵ 5700 M^{-1} cm^{-1}).

[Ru$_2$(OH)$_2$(bpy)$_2$(btpyan)](SbF$_6$)$_2$·3H$_2$O. A suspension of MeOH/H_2O (9/1 v/v, 30 mL) containing [Ru_2Cl_6(btpyan)] (100 mg, 0.095 mmol) and 2,2′-bipyridine (30 mg, 0.19 mmol) was deoxygenated with a stream of dinitrogen for 30 min. An MeOH solution of AcOK (186 mg, 1.9 mmol) was then added by syringe to the MeOH/H_2O suspension. The reaction mixture was stirred for 1 day at room temperature under nitrogen, during which [Ru_2Cl_6(btpyan)] gradually dissolved into the solvent and the solution became reddish brown. After concentration of the solution to ca. 5 mL by evaporation under reduced pressure, 15 mL of acetone was added and AcOK was filtered off. [Ru_2(OH)$_2$(bpy)$_2$(btpyan)](AcO) was purified by column chromatography using Alumina A-super I (ICN Biomedicals GmbH) and acetone as the eluent. An aqueous solution of $NaSbF_6$ was added to the brown fraction, followed by evaporation of acetone from the mixture to give a brown powder. Yield: 32 mg (25%). Anal. Calcd for $C_{64}H_{46}O_2N_{10}F_{12}Ru_2Sb_2$·$3H_2O$: C, 44.83; H, 3.06; N, 8.17. Found: C, 44.48; H, 3.23; N, 7.93. ESI-MS: m/z 595 ([Ru_2(OH)$_2$(bpy)$_2$(btpyan)]$^{2+}$). Electronic absorption data (MeOH solution): λ_{max} 498 nm (ϵ 13 800 M^{-1} cm^{-1}).

X-ray Structure Determination of BTPYAN. BTPYAN was recrystallized from chloroform/hexane (1/1 v/v) in the dark at room temperature for 3 weeks, and small pale yellow crystals were obtained. A prism-shaped crystal (0.38 × 0.25 × 0.15 mm) was glued to the tip of a glass capillary in the air, and data were collected on a Bruker SMART Platform diffractometer with a CCD detector. SMART software was used for data acquisition, and SAINT software, for data extraction.[8] The crystallographic data are presented in Table 1. All the calculations were performed with the teXsan crystallographic software

Table 1. Crystal Parameters and X-ray Diffraction Data for BTPYAN

empirical formula	$C_{44}H_{28}N_6$	γ/deg	90
fw	640.75	V/Å^3	3255(2)
space group	$C2/c$ (No. 15)	Z	4.00
a/Å	18.6820(48)	T/°C	23
b/Å	11.6855(29)	ρ_{calc}/g cm^{-3}	1.307
c/Å	14.9353(42)	μ/cm^{-1}	0.787
α/deg	90	R^a	0.1180
β/deg	93.3360(85)	$R_w{}^b$	0.0730

^{a} $R = \sum||F_o| - |F_c||/\sum|F_o|$. ^{b} $R_w = [\sum w(|F_o| - |F_c|)^2/\sum wF_o^2]^{1/2}$; $w = 1/\sigma^2(F_o)$.

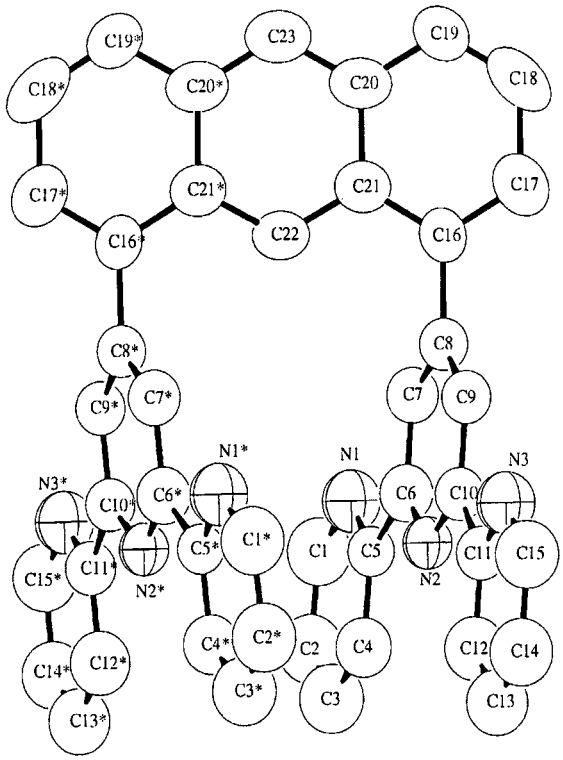

Figure 1. Molecular structure of BTPYAN.

package.[9] The structure was solved by direct methods using the program MITHRIL90.[10] C atoms of anthracene were placed in anisotropically refined positions, other non-hydrogen atoms were placed in isotropically refined positions, and the hydrogen atoms were placed in calculated positions. The R value was not sufficiently low because the crystal of BTPYAN was too small to obtain suitable reflections. However, it was confirmed by X-ray crystal structure analysis that BTPYAN has the structure shown in Figure 1.

Instrumental Measurements. ^{1}H NMR spectra were obtained on a JEOL JMN-La500 Lambda FT-NMR system, ESI-MS on a PE SCIEX API300, and electronic absorption spectra on a Shimadzu UV-3100PC UV−vis−NIR scanning spectrophotometer.

Cyclic voltammetric experiments were carried out in a one-compartment cell containing of an Ag/AgCl reference electrode, a glassy carbon or a platinum working electrode, and a platinum counter electrode. Each test solution was deoxygenated with a stream of N_2. ^{t}BuOK and $HClO_4$ were used as the base and acid, respectively. An ALS/Chi model 660 electrochemical analyzer was used to collect the cyclic voltammetric data.

Spectroelectrochemistry was performed with a thin-layer electrode cell with a platinum minigrid working electrode sandwiched between two glass sides of an optical cell (path length 0.5 mm), where an Ag/AgCl reference electrode was separated from the working compartment by a luggin capillary.

Water oxidation was conducted by using a glass cell composed of three compartments under controlled-potential-electrolysis conditions.[11] Working and counter electrode compartments were separated by a cation-exchange membrane (Nafion 117, Aldrich Chemical Co., Inc.). An Ag/AgCl reference electrode was separated from the working compartment by a luggin capillary. Platinum plates were washed with dilute aqueous HNO_3 and water and employed as working and counter electrodes. CF_3CH_2OH (15 mL) was used as the solvent and deoxygenated by bubbling with He. A Hokuto Denko HA-151 potentiostat/function generator was used. The amount of electricity was measured with a Hokuto Denko HF-201 Coulomb/Ampere Meter. At a fixed interval of coulombs consumed in the oxidation of water, each 0.1 cm^3 portion of gas was sampled from the gaseous phase of the working electrode compartment with a pressure-locked syringe. Dioxygen was quantitatively and qualitatively analyzed by using a GC instrument (Shimadzu GC-8A) equipped with a 1 m column filled with Molecular Sieve 13X using He as the carrier gas and GC-MS instrument (Shimadzu GCMS-QP 1000EX), respectively.

Cyclic Voltammetric Measurements and Controlled-Potential Electrolysis Using a Complex-Modified ITO Electrode. A complex-modified ITO electrode was prepared as follows: An ITO electrode was washed with an ultrasonic cleaner for 30 min, successively, in water containing a neutral detergent, acetone, and MeOH and then dried at room temperature. An acetone solution of the complex (5.0×10^{-4} mol/L) was dropped on the cleansed electrode by using a microsyringe, and the complex-modified electrode was dried at room temperature.

Cyclic voltammetric experiments were carried out in a one-compartment cell containing of an Ag/AgCl reference electrode; 2.0 cm^2 of an ITO glass plate modified with the complex (1.2×10^{-8} mol) and a platinum wire were used as the working electrode and the counter electrode, respectively. A KOH/H_3PO_4 aqueous solution (0.1 M) was used as the solvent, whose pH was controlled by the addition of an aqueous solution of KOH or H_3PO_4.

Water oxidation was carried out under controlled-potential-electrolysis conditions in an aqueous buffer solution (pH 4.0, H_3PO_4/KOH, 1.0 M) at room temperature under an He atmosphere with the use of an electrolysis cell consisting of three compartments: one for the complex-modified ITO electrode (2.0×10^{-8} mol/10.0 cm^2), the second for a platinum counter electrode (2.0 cm^2), which was separated from the complex-modified ITO electrode by a cation-exchange membrane (Nafion 117, Aldrich Chemical Co., Inc.), and the third for an Ag/AgCl reference electrode. Evolved O_2 analysis was carried under similar conditions with the reaction mixture in a CF_3CH_2OH solution.

Results and Discussion

Synthesis and Structure of 1,8-Bis(2,2′:6′,2″-terpyridyl)-anthracene (BTPYAN). The Kröhnke-type[12] synthesis of BTPYAN is outlined in Scheme 1. Aldol condensation of 2-acetylpyridine with 1,8-diformylanthracene in a 2/1 ratio afforded enone **A** as a yellow solid. The subsequent Michael reaction of **A** with 2-acetylpyridine generated bis(dionyl)-anthracene **B**, which was ring-closed with ammonium acetate to give BTPYAN in 38% yield (two steps). An alternative reaction of 4 equiv of 2-acetylpyridine with diformylanthracene did not give bis(dionyl)anthracene **B** (exemplified by the preparations of 4,4′,4″-triphenylterpyridine,[13] 4′-ferrocenylterpyridine,[14] and 4-phenylterpyridine[15]). After purification by HPLC, recrystallization of BTPYAN from $CHCl_3$/hexane gave

(8) *SMART and SAINT V-4 Programs*; Bruker Analytical X-ray Systems Inc.: Madison, WI, 1996.
(9) *teXsan*: *Single Crystal Structure Analysis Software*, Version 1.6; Molecular Structure Corp.: The Woodlands, TX, 1993.
(10) *MITHRIL90*: *Computer Programs for Automatic Solution of Crystal Structures from X-ray Diffraction Data*; Gilmore, C. J., Ed.; University of Glasgow: Glasgow, Scotland, 1990.
(11) For details of the electrolysis cell used in this study, see: Ishida, H.; Tanaka, K.; Tanaka, T. *Organometallics* **1987**, *6*, 181.
(12) Kröhnke, F. *Synthesis* **1976**, 1.
(13) Beley, M.; Collin, J.-P.; Sauvage, J.-P. *J. Am. Chem. Soc.* **1985**, *107*, 1138.
(14) Constable, E. C.; Edwards, A. J.; Martínez-Máñez, R.; Raithby, P. R.; Cargill Thompson, A. M. W. *J. Chem. Soc., Dalton Trans.* **1994**, 645.

Scheme 1. Synthesis of BTPYAN

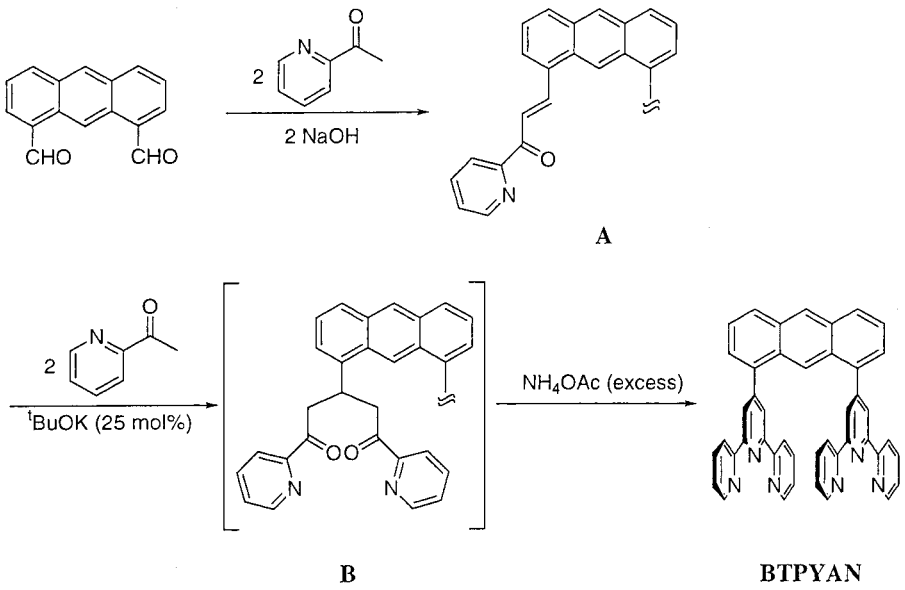

Scheme 2. Synthesis of the Quinone Complex [**1**](SbF$_6$)$_2$

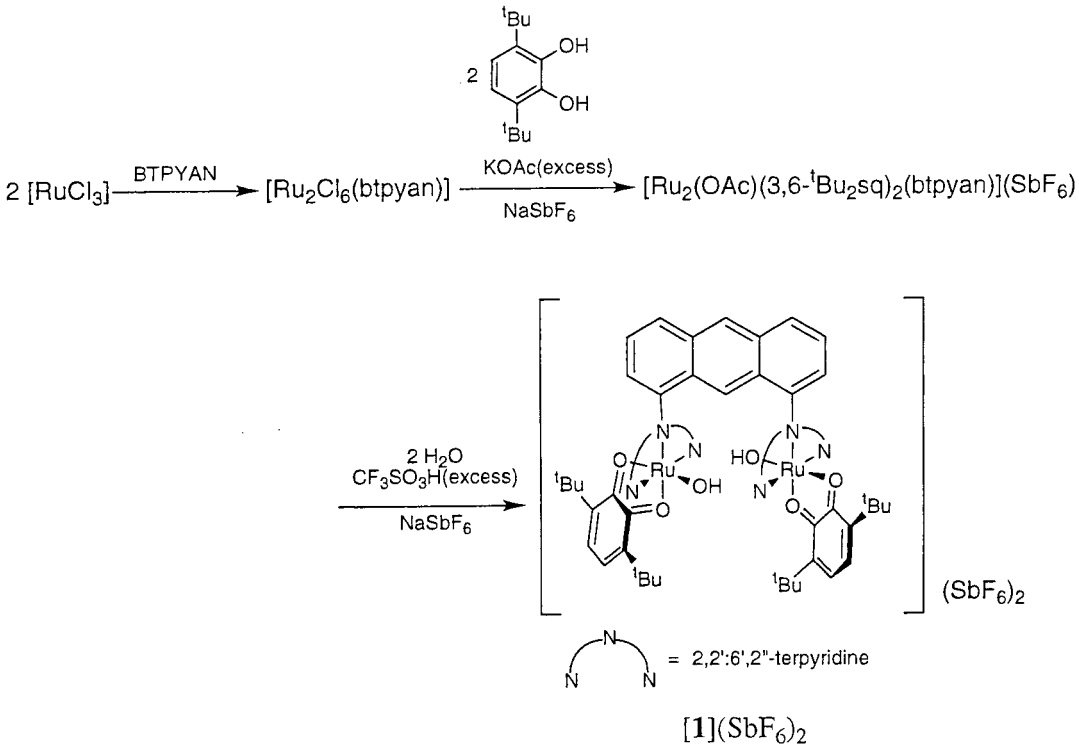

pale yellow crystals. The crystal structure of BTPYAN was determined by X-ray analysis (Figure 1). The two terpyridyl groups linked to the 1,8-positions of anthracene are located face-to-face and are parallel. BTPYAN has a rotation axis that includes C22 and C23, and the two terpyridyl groups are crystallographically equivalent in the crystal structure. The dihedral angles between anthracene and the terpyridines are 69.06°. Free rotation of the two terpyridyl groups must be inhibited because of these steric repulsions. The short distance of 4.22 Å between two central N atoms of two terpyridyl groups (N2 and N2*) compared with that of 4.88 Å between C16 and C16* of anthracene is explained by the $\pi-\pi$ stacking of the two terpyridyl groups. The distance between two metals, therefore, is estimated to be in the range 4−5 Å when BTPYAN forms a dinuclear complex.

Syntheses of the Dinuclear Complexes. The synthesis of the dinuclear quinone complex [**1**](SbF$_6$)$_2$, outlined in Scheme 2, was similar to that of [Ru(OH$_2$)(3,5-^{t}Bu$_2$qui)(terpy)](ClO$_4$)$_2$.[16] The reaction of [Ru$_2$Cl$_6$(btpyan)] with 3,6-di-*tert*-butylcatechol in the presence of KOAc (excess) gave the acetato complex. ESI-MS measurements and elemental analysis of the acetato complex indicated a monocationic diruthenium complex bridged by btpyan and acetato ligands. Electronic absorption spectra of

(15) Constable, E. C.; Lewis, J.; Liptrot, M. C.; Raithby, P. R. *Inorg. Chim. Acta* **1990**, *178*, 47.

(16) (a) Tsuge, K.; Kurihara. M.; Tanaka, K. *Chem. Lett.* **1998**, 1069. (b) Tsuge, K.; Kurihara, M.; Tanaka, K. *Bull. Chem. Soc. Jpn.* **2000**, *73*, 607.

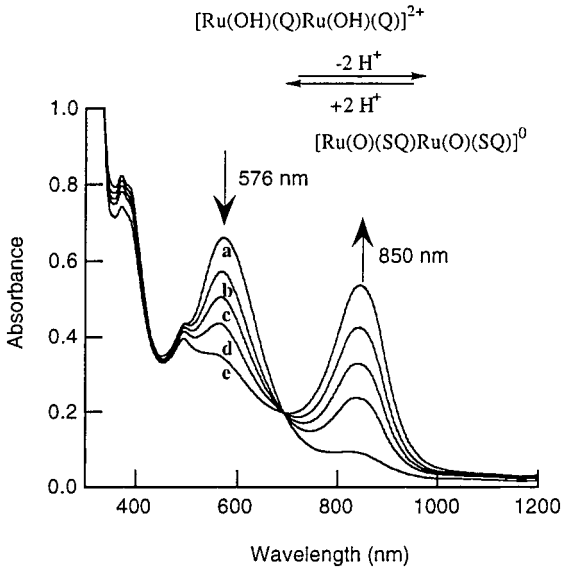

Figure 2. Electronic absorption spectra of [**1**](SbF$_6$)$_2$ in MeOH and in the presence of various amounts of ^{t}BuOK: 0 equiv (a); 0.5 equiv (b); 1.0 equiv (c); 1.5 equiv (d); 2.0 equiv (e).

the acetato complex in MeOH showed a strong band at 845 nm, which was assigned to the metal-to-ligand charge-transfer (MLCT) band resulting from the ruthenium(II)−semiquinone moiety on the basis of the electronic spectra of mononuclear ruthenium−quinone complexes.[16−18] Hydrolysis of the acetato complex produced the quinone complex [**1**]$^{2+}$ with two hydroxo ligands but not with the aqua ligands (vide infra), and the hydroxo complex was isolated as [**1**](SbF$_6$)$_2$. Electronic absorption spectra of [**1**](SbF$_6$)$_2$ in MeOH displayed a strong band at 576 nm assignable to the MLCT band of the ruthenium(II)−quinone moiety.[16−18] The electronic structure of [**1**]$^{2+}$, therefore, is expressed as [Ru^{II}(OH)(Q)Ru^{II}(OH)(Q)]$^{2+}$ (Q = 3,6-di-*tert*-butyl-1,2-quinone) rather than [Ru^{III}(OH)(SQ)Ru^{III}(OH)(SQ)]$^{2+}$ (SQ = 3,6-di-*tert*-butyl-1,2-semiquinone). On the basis of the crystal structure of BTPYAN, the two hydroxo groups in [**1**]$^{2+}$ could be adjacently located face-to-face inside the cavity formed by the two terpyridyls and the two bulky 3,6-di-*tert*-butyl-1,2-quinones, as shown in Scheme 2.[19] The bipyridine analogue of [**1**](SbF$_6$)$_2$ was synthesized by a method similar to the preparation of [**1**](SbF$_6$)$_2$. We also prepared [Ru$_2$(OH)$_2$(bpy)$_2$(btpyan)](SbF$_6$)$_2$ ([**2**](SbF$_6$)$_2$) as a bipyridine analogue of [**1**](SbF$_6$)$_2$ to compare the redox behaviors of the quinone and bipyridine ligands in the dinuclear Ru complexes. [**2**](SbF$_6$)$_2$ was characterized by ESI-MS and elemental analysis (see the Experimental Section).[19]

The Acid-Base Equilibrium and Redox Properties of [1]$^{2+}$ and [2]$^{2+}$. Electronic absorption spectra of [**1**](SbF$_6$)$_2$ in MeOH showed a strong band at 576 nm. Addition of ^{t}BuOK to the solution resulted in the appearance of a new band at 850 nm, which gradually increased with an increase in the amount of ^{t}BuOK at the expense of the band at 576 nm (Figure 2). The 576 nm band completely disappeared in the presence of 2.0 equiv of ^{t}BuOK, and further addition of ^{t}BuOK did not cause any spectral changes. Moreover, acidification of the resultant purple solution by the addition of 2.0 equiv of HClO$_4$ resulted in the complete restoration of the 576 nm band and disappearance of the 850 nm band. The 576 and the 850 nm bands are reasonably assigned to the MLCT bands of the Ru(II)−quinone and Ru(II)−semiquinone moieties, respectively.[16] Such a reversible change of the electronic absorption spectra is attributable to the occurrence of the acid−base equilibrium between [Ru(OH)(Q)Ru(OH)(Q)]$^{2+}$ and [Ru(O)(SQ)Ru(O)(SQ)]$^{2+}$ (eq 2).

$$[\mathrm{Ru(OH)(Q)Ru(OH)(Q)}]^{2+} \underset{+2\mathrm{H}^+}{\overset{-2\mathrm{H}^+}{\rightleftharpoons}} [\mathrm{Ru(O)(SQ)Ru(O)(SQ)}]^{0} \quad (2)$$

It is worthy of note that the dissociation of two protons of [Ru^{II}(OH)(Q)Ru^{II}(OH)(Q)]$^{2+}$ produces [Ru^{II}(O)(SQ)Ru^{II}(O)(SQ)]^0 and not [Ru^{II}(O)(Q)Ru^{II}(O)(Q)]^0.[20] Thus, deprotonation of the hydroxo groups is coupled with the redox reaction of the quinones. The acid−base equilibrium of the OH$_2$ group of [Ru(OH$_2$)(Q)(terpy)]$^{2+}$ is also coupled with the reduction of quinone to semiquinone in acetone.[16] On the other hand, the electronic absorption spectrum of the analogous dinuclear bipyridine complex [**2**](SbF$_6$)$_2$ in MeOH showed no change upon the addition of a 10 molar excess of ^{t}BuOK. The distinct difference in the acidities of the hydroxo protons of [**1**]$^{2+}$ and [**2**]$^{2+}$ is correlated with the π^* orbitals of the quinone ligands and bipyridyl ligands of the complexes. Intramolecular electron transfer from the negatively charged oxo ligands, formed by dissociation of the hydroxo protons, to the low-lying π^* orbitals of the quinones of [**1**]$^{2+}$ must be much easier than that to the π^* orbitals of the polypyridyls of [**2**]$^{2+}$ on the basis of the ligand-localized redox reactions of both complexes (vide infra).

The cyclic voltammogram (CV) of [**1**](SbF$_6$)$_2$ in MeOH shows four anodic and cathodic waves in a potential range from +0.8 to −1.0 V (vs Ag/AgCl; Figure 3). The four nearly reversible redox couples observed at $E_{1/2}$ = +0.43, +0.35, −0.47, and −0.56 V with a peak separation of ΔE_p ($=E_{ap} - E_{pc}$) of 80, 93, 90, and 102 mV, respectively, are associated with the ligand-localized reductions of the two quinones on the basis of the rest potential of [**1**]$^{2+}$ (+0.49 V) in the same solvent. [**2**]$^{2+}$ showed no polypyridyl-localized redox reactions up to −1 V. The redox potentials at $E_{1/2}$ = +0.43 and +0.35 V, therefore, were ascribed to the reductions of the quinones to semiquinones in the case of [**1**]$^{2+}$, involving the [Ru(OH)(Q)Ru(OH)(Q)]$^{2+}$/[Ru(OH)(Q)Ru(OH)(SQ)]$^{+}$/[Ru(OH)(SQ)Ru(OH)(SQ)]^0 redox couples, and the remaining two redox potentials at $E_{1/2}$ = −0.40 and −0.56 V were ascribed to the reductions of the semiquinones to catecholates involving the [Ru(OH)(SQ)Ru(OH)(SQ)]^0/[Ru(OH)(SQ)Ru(OH)(C)]$^-$/[Ru(OH)(C)Ru(OH)(C)]$^{2-}$ couples (C = 3,6-di-*tert*-butylcatecholate). The addition of 2.0 equiv of ^{t}BuOK to the MeOH solution of [**1**]$^{2+}$ shifted the rest potential of the solution from +0.49 to −0.12 V, ascribable to the conversion from [Ru(OH)(Q)Ru(OH)(Q)]$^{2+}$ to [Ru(O)(SQ)Ru(O)(SQ)]^0 (eq 2) (Figure 3b). In accordance with the formation of [Ru(O)(SQ)Ru(O)(SQ)]^0, two semiquinone ligands of the complex underwent two successive oxidations, affording [Ru(O)(SQ)Ru(O)(Q)]$^+$ and [Ru(O)(Q)-

(17) Kurihara, M.; Daniele, S.; Tsuge, K.; Sugimoto, H.; Tanaka, K. *Bull. Chem. Soc. Jpn.* **1998**, *71*, 867.
(18) (a) Haga, M.; Dodsworth, E. S.; Lever, A. B. P. *Inorg. Chem.* **1986**, *25*, 447. (b) Cox, D. D.; Que, L., Jr. *J. Am. Chem. Soc.* **1988**, *110*, 8085. (c) Bhattacharya, S.; Boone, S. R.; Fox, G. A.; Pierpont, C. G. *J. Am. Chem. Soc.* **1990**, *112*, 1088. (d) Masui, H.; Lever, A. B. P.; Auburn, P. R. *Inorg. Chem.* **1991**, *30*, 2402.
(19) Modelings of [**1**]$^{2+}$ and [**2**]$^{2+}$ demonstrated that two coordinated OH groups are sterically forced to be juxtaposed within the cavity by btpyan and the two 3,6-di-*tert*-butylquinone or 2,2′-bipyridine groups.
(20) Deprotonation of the Ru^{II}(OH)$^-$ group of [**1**]$^{2+}$ causes the reduction of the Ru^{II}(Q) moiety to Ru^{II}(SQ) owing to intramolecular electron transfer from the resultant O^{2-} to Q. So, either two Ru^{II}−O$^{\bullet-}$ bonds or an Ru^{II}−O−O−Ru^{II} arrangement would be formed in the deprotonated form of [**1**]$^{2+}$. However, FT-Raman and resonance Raman spectra (irradiated at 850 nm for the MLCT band) showed no relevant signals for these bonds. As the electronic structure of the oxo ligands of the deprotonated form of [**1**]$^{2+}$ was not clear in the present study, the deprotonated form of [**1**]$^{2+}$ is simply given as [Ru^{II}(O)(SQ)Ru^{II}(O)(SQ)]^0.

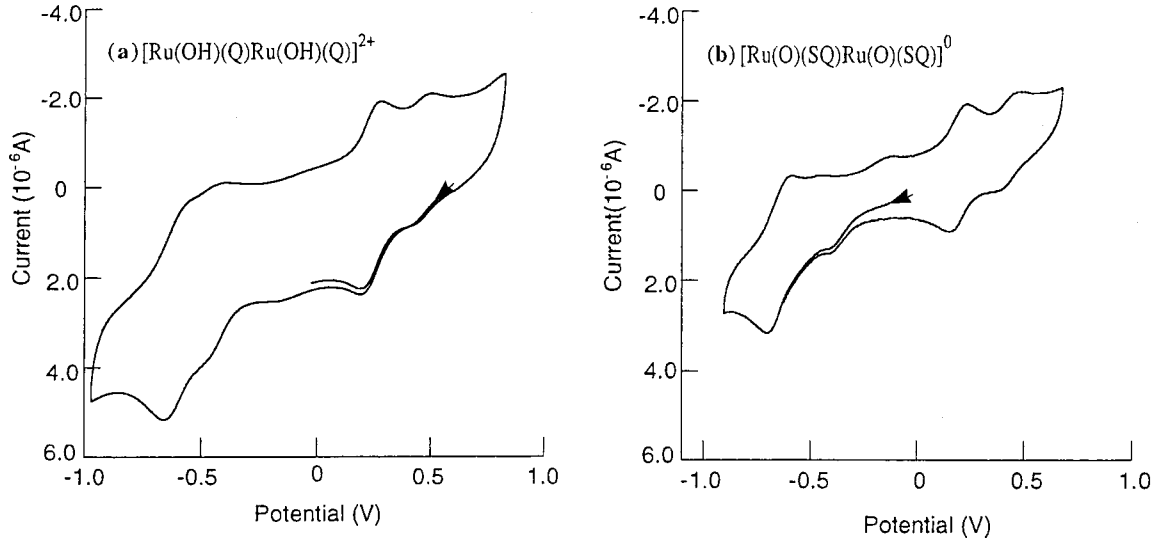

Figure 3. Cyclic voltammograms of [**1**]$(SbF_6)_2$ in the absence (a) and the presence of 2.0 equiv of ^{t}BuOK (b) in MeOH under N_2 atmosphere. The arrows indicated the rest potentials of the solution and the direction of scans.

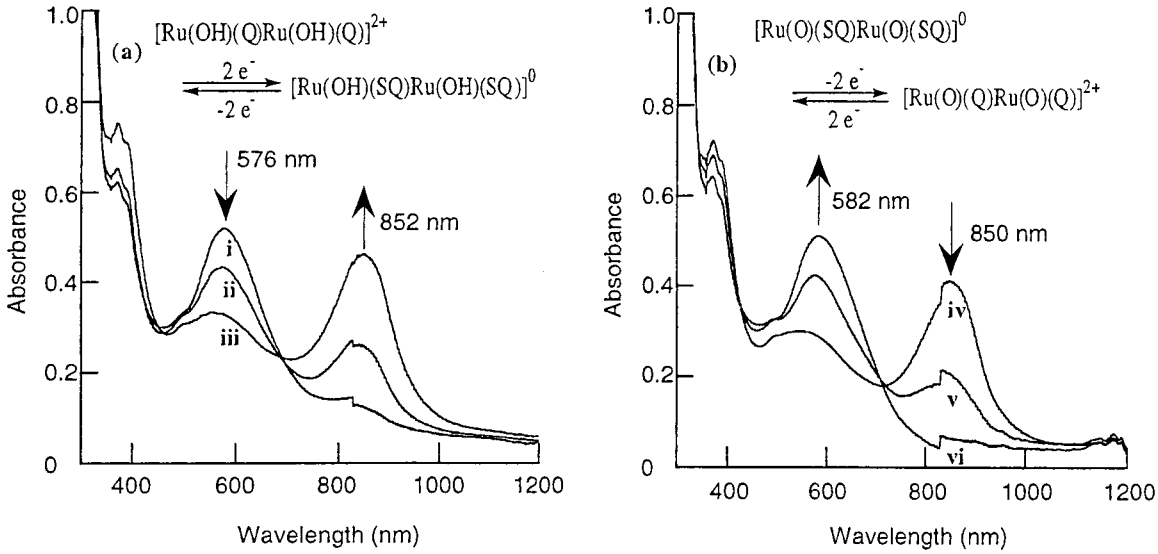

Figure 4. Electronic absorption spectra of [**1**]$(SbF_6)_2$ (a) before electrolysis (i) and after electrolysis at +0.38 V (ii) and −0.05 V (iii) and of $[Ru(O)(SQ)Ru(O)(SQ)]^0$ generated from [**1**]$(SbF_6)_2$ with 2.0 equiv of ^{t}BuOK (b) before electrolysis (iv) and after the electrolysis at +0.35 V (v) and +0.55 V (vi).

$Ru(O)(Q)]^{2+}$ at $E_{1/2}$ = +0.30 and +0.40 V, respectively, and also two successive reductions, producing $[Ru(O)(SQ)Ru(O)(C)]^-$ and $[Ru(O)(C)Ru(O)(C)]^{2-}$ at E_{pc} = −0.43 and −0.68 V, respectively. Besides the pair of cathodic and anodic waves of the $[Ru(O)(SQ)Ru(O)(C)]^-/[Ru(O)(C)Ru(O)(C)]^{2-}$ couple at E_{pc} = −0.68 V and E_{pa} = −0.58 V, there is a weak anodic wave at E_{pa} = −0.45 V, which may result from partial degradation of $[Ru(O)(C)Ru(O)(C)]^{2-}$.

To confirm the ligand-localized redox reaction of $[\mathbf{1}]^{2+}$ coupled with the acid−base equilibrium of the hydroxo ligands, electronic absorption spectra of $[\mathbf{1}]^{2+}$ were recorded under electrolysis conditions (Figure 4). Electrochemical reduction of [**1**]$(SbF_6)_2$ at +0.38 V in MeOH caused a decrease in the MLCT band at 576 nm and the appearance of a new band at 852 nm (ii in Figure 4a) in MeOH. The 576 nm band disappeared and the 852 nm band increased upon the shift of the electrolysis potential from +0.38 to −0.05 V (iii in Figure 4a). On the basis of the MLCT bands of the Ru(II)−quinone and Ru(II)−semiquinone moieties at 576 and 852 nm, respectively, $[\mathbf{1}]^{2+}$ must be reduced to $[Ru(OH)(SQ)Ru(OH)(Q)]^+$ and $[Ru(OH)(SQ)Ru(OH)(SQ)]^0$ at +0.43 V and at +0.45 V, respectively (eq 3). On the other hand, the strong absorption band at 850 nm of $[Ru(O)(SQ)Ru(O)(SQ)]^0$ developed by the treatment of [**1**]$(SbF_6)_2$ with 2 equiv of ^{t}BuOK weakened upon the electrochemical oxidation of the solution at +0.35 V and a new band

$$[\mathbf{1}]^{2+} \underset{+0.43\ \mathrm{V}}{\overset{e^-}{\rightleftharpoons}} [Ru(OH)(SQ)Ru(OH)(Q)]^+ \underset{+0.35\ \mathrm{V}}{\overset{e^-}{\rightleftharpoons}} [Ru(OH)(SQ)Ru(OH)(SQ)]^0 \quad (3)$$

appeared at 582 nm (Figure 4b). The 850 nm band completely disappeared and the band at 582 nm further increased upon electrolysis at +0.55 V. The spectral changes of $[Ru(O)(SQ)Ru(O)(SQ)]^0$ upon electrolysis at +0.35 and +0.55 V also must result from the formation of $[Ru(O)(SQ)Ru(O)(Q)]^+$ and $[Ru(O)(Q)Ru(O)(Q)]^{2+}$, respectively. The redox potentials at $E_{1/2}$ = +0.40 and +0.30 V, therefore, were assigned to the redox reactions of the $[Ru(O)(Q)Ru(O)(Q)]^{2+}/[Ru(O)(SQ)Ru(O)(Q)]^+$

$$[Ru(O)(Q)Ru(O)(Q)]^{2+} \underset{+0.40\ \mathrm{V}}{\overset{e^-}{\rightleftharpoons}} [Ru(O)(Q)Ru(O)(SQ)]^+ \underset{+0.30\ \mathrm{V}}{\overset{e^-}{\rightleftharpoons}} [Ru(O)(SQ)Ru(O)(SQ)]^0 \quad (4)$$

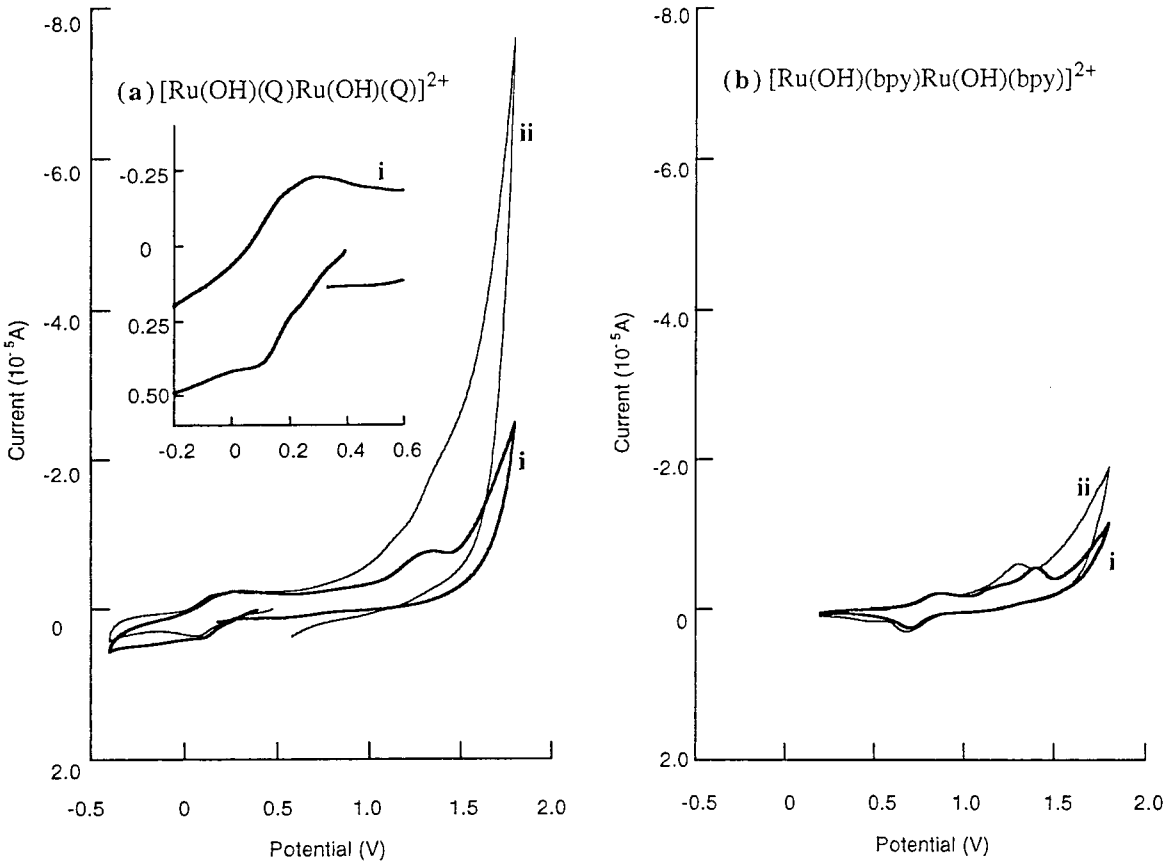

Figure 5. Cyclic voltammograms of [**1**]$(SbF_6)_2$ (a) and [**2**]$(SbF_6)_2$ (b) in the absence (i) and the presence of water (10 v/v%) (ii) in CF_3CH_2OH/ether (1/1 v/v) solution. Inset: magnification of the potential range from −0.2 to +0.6 V.

couple and the $[Ru(O)(Q)Ru(O)(SQ)]^+/[Ru(O)(SQ)Ru(O)(SQ)]^0$ couple (eq 4).

Water Oxidation Catalyzed by the Quinone Complex [1]$(SbF_6)_2$ and the Bipyridine Complex [2]$(SbF_6)_2$ in Solutions. Both $[\mathbf{1}]^{2+}$ and $[\mathbf{2}]^{2+}$ were soluble in MeOH and acetone. These solvents, however, undergo irreversible oxidations at potentials more positive than 1.0 V (vs Ag/AgCl). Thus, the CVs of [**1**]$(SbF_6)_2$ and [**2**]$(SbF_6)_2$ were measured up to +1.8 V in 2,2,2-trifluoroethanol/ether (50/50 v/v) to detect the metal-centered Ru^{II}/Ru^{III} redox couples of these complexes (Figure 5). Indeed, a broad irreversible anodic wave appeared at $E_p = +1.34$ V, in addition to waves for the reversible $[Ru^{II}(OH)(Q)Ru^{II}(OH)(Q)]^{2+}/[Ru^{II}(OH)(SQ)Ru^{II}(OH)(Q)]^+$ and $[Ru^{II}(OH)(SQ)Ru^{II}(OH)(Q)]^+/[Ru^{II}(OH)(SQ)Ru^{II}(OH)(SQ)]^0$ redox couples at $E_{1/2} = +0.26$ and +0.15 V, respectively. The area of the broad anodic wave at +1.34 V was almost same as the total area of the two anodic waves at $E_{1/2} = +0.26$ and +0.15 V. In addition, controlled-potential electrolysis of $[\mathbf{1}]^{2+}$ at +1.60 V consumed two electrons per $[\mathbf{1}]^{2+}$ complex in CF_3CH_2OH/ether. Thus, the broad anodic wave at +1.34 V involves the two redox reactions of the $[Ru^{II}(OH)(Q)Ru^{II}(OH)(Q)]^{2+}/[Ru^{II}(OH)(Q)Ru^{III}(OH)(Q)]^{3+}$ couple and the $[Ru^{II}(OH)(Q)Ru^{III}(OH)(Q)]^{3+}/[Ru^{III}(OH)(Q)Ru^{III}(OH)(Q)]^{4+}$ couple (eq 5).[21] Addition of H_2O to the

$$[Ru^{II}(OH)(Q)Ru^{II}(OH)(Q)]^{2+} \xrightarrow[+1.34\ V]{-2e^-} [Ru^{III}(OH)(Q)Ru^{III}(OH)(Q)]^{4+} \quad (5)$$

solution (10%) caused strong catalytic currents at potentials more positive than +1.0 V, suggesting that either $[Ru^{III}(OH)(Q)Ru^{III}(OH)(Q)]^{4+}$ or the oxidized form has an ability to oxidize water. In fact, the controlled-potential electrolysis of [**1**]$(SbF_6)_2$ (1.5 μmol) in trifluoroethanol containing water (10%) at +1.70 V evolved 0.69 mL of dioxygen with a current efficiency of 91% (21 turnovers). During the progress of water oxidation, the presence of $[\mathbf{1}]^{2+}$ in the solution was evidenced in the ESI-MS and electronic spectra. On the other hand, $[\mathbf{1}]^{2+}$ was not confirmed in the ESI-MS and electronic spectra of the solution after the catalytic currents had completely stopped.[22] In harmony with this, no anodic current flowed in the absence of [**1**]$(SbF_6)_2$ under similar reaction conditions. Thus, it is concluded that the oxidized form of $[\mathbf{1}]^{2+}$ is the active species for water oxidation.

The bipyridine complex [**2**]$(SbF_6)_2$ displayed only the metal-centered redox reactions; the reversible redox couple at $E_{1/2} = +0.79$ V ($\Delta E_p = 180$ mV) and the irreversible anodic wave at $E_p = +1.43$ V are probably attributable to the $[Ru^{II}(OH)(bpy)Ru^{II}(OH)(bpy)]^{2+}/[Ru^{III}(OH)(bpy)Ru^{III}(OH)(bpy)]^{4+}$ and $[Ru^{III}(OH)(bpy)Ru^{III}(OH)(bpy)]^{4+}/[Ru^{IV}(OH)(bpy)Ru^{IV}(OH)(bpy)]^{6+}$ redox couples (eq 6). The pair of the anodic and

$$[Ru^{II}(OH)(bpy)Ru^{II}(OH)(bpy)]^{2+} \underset{+0.79\ V}{\overset{-2e^-}{\rightleftharpoons}} [Ru^{III}(OH)(bpy)Ru^{III}(OH)(bpy)]^{4+} \xrightarrow[+1.43\ V]{-2e^-} [Ru^{IV}(OH)(bpy)Ru^{IV}(OH)(bpy)]^{6+} \quad (6)$$

cathodic waves of the $[Ru^{II}(OH)(bpy)Ru^{II}(OH)(bpy)]^{2+}/[Ru^{III}(OH)(bpy)Ru^{III}(OH)(bpy)]^{4+}$ redox couple at $E_{1/2} = +0.79$ V

(21) Mononuclear $[Ru(OH_2)(Q)(terpy)]^{2+}$ and $[RuX(Q)(terpy)]^+$ (X = Cl, $OCOCH_3$) also displayed an irreversible anodic wave for the Ru^{II}/Ru^{III} redox couple around +1.3 V. The oxidation−reduction cycle of [**1**]$(SbF_6)_2$ upon electrolysis at +1.60 V and subsequent electrolysis at +0.5 V in CF_3CH_2OH did not result in the recovery of the electronic absorption spectrum of $[\mathbf{1}]^{2+}$. Thus, $[Ru^{III}(OH)(Q)Ru^{III}(OH)(Q)]^{4+}$ is not stable in the absence of water.

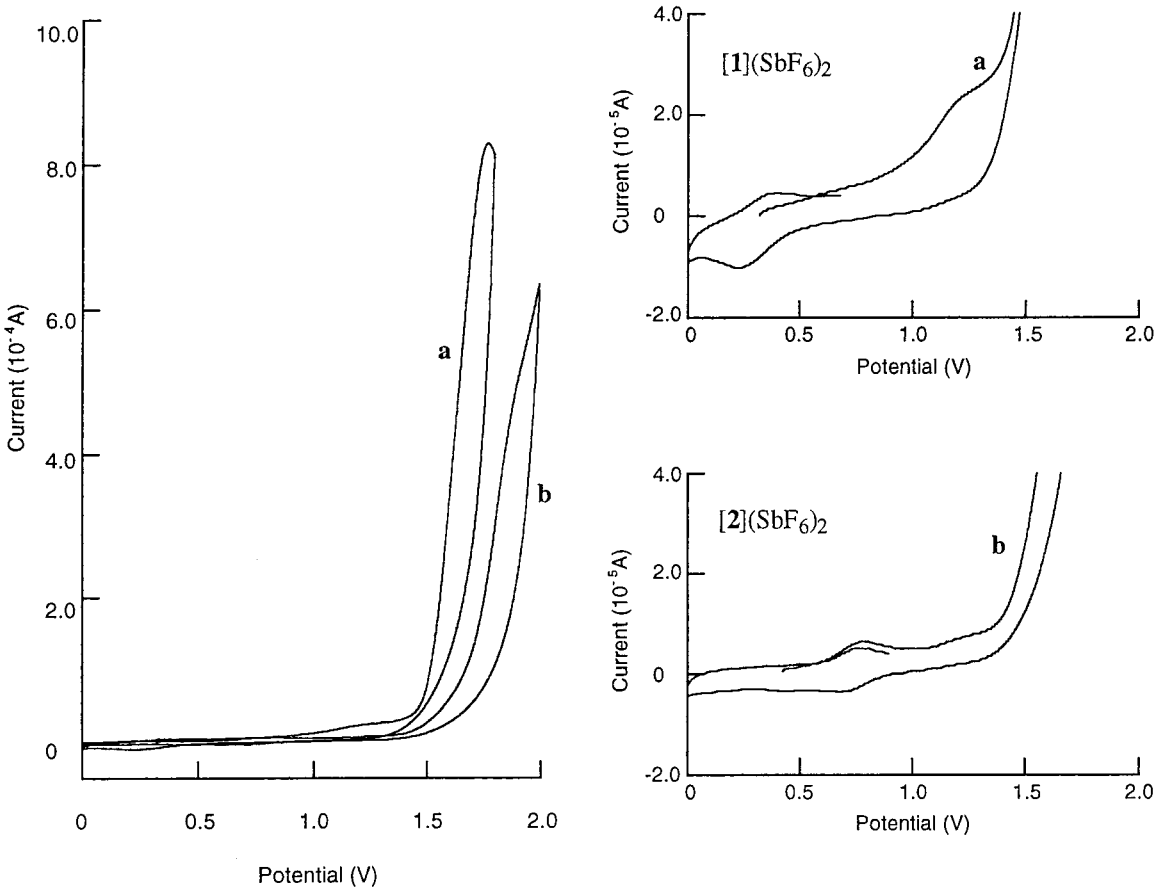

Figure 6. Cyclic voltammograms of [**1**]$(SbF_6)_2$ (a) and [**2**]$(SbF_6)_2$ (b) modified on an ITO electrode in KOH/H_3PO_4 aqueous solution at pH 4.0. Magnifications of CVs a and b are depicted at the right.

were not influenced by an addition of H_2O to the solution, while the irreversible anodic wave at $E_{pa} = +1.43$ V shifted to $E_{pa} = +1.31$ V in CF_3CH_2OH/H_2O (9/1 v/v). This observation suggests that $[Ru^{III}(OH)(bpy)Ru^{III}(OH)(bpy)]^{4+}$ does not dissociate protons on the cyclic voltammetric time scale and that oxidation of $[Ru^{III}(OH)(bpy)Ru^{III}(OH)(bpy)]^{4+}$ is accompanied by proton dissociation. An increase of irreversible anodic currents at potentials more positive than the anodic wave at $E_{pa} = +1.31$ V indicates that the oxidation product of $[\mathbf{2}]^{4+}$ has the ability to promote water oxidation in CF_3CH_2OH/H_2O, although the irreversible currents are much smaller than those of $[\mathbf{1}]^{2+}$.

Water Oxidation Using ITO (Indium−Tin−Oxide) Electrodes Modified with [1](SbF$_6$)$_2$ and [2](SbF$_6$)$_2$. As mentioned above, the quinone ligands of $[\mathbf{1}]^{2+}$ were spontaneously reduced upon dissociation of the hydroxo protons in CH_3OH. The redox behaviors of [**1**]$(SbF_6)_2$ and [**2**]$(SbF_6)_2$ modified on an ITO electrode and glass plate were examined at various pHs in H_2O by taking advantage of the insolubility of [**1**]$(SbF_6)_2$ and [**2**]$(SbF_6)_2$. The solid state of [**1**]$(SbF_6)_2$ modified on a glass plate also exhibited a strong MLCT band at 578 nm in water at pHs less than 2.0. The band intensity at 578 nm gradually decreased above pH 2.0. At the same time, a new band emerged at 850 nm and its intensity increased up to pH 3.0. This pH-dependent spectral change of [**1**]$(SbF_6)_2$ modified on a glass plate was essentially same as that in MeOH in the absence and the presence of ^{t}BuOK. Thus, [**1**]$(SbF_6)_2$ modified on the glass plate was also smoothly converted to $[Ru(O)(SQ)Ru(O)(SQ)]^0$ at pHs higher than 3.0 owing to the dissociation of protons. The CV of [**1**]$(SbF_6)_2$ modified on an ITO electrode (1.2×10^{-8} mol/2.0 cm^2) in water (pH 4.0) exhibits a broad redox wave centered at +0.32 V (vs Ag/AgCl), an irreversible anodic wave at +1.19 V, and a strong anodic current at potentials more positive than +1.2 V (Figure 6a). On the basis of the redox behavior of the complex in MeOH and the electronic absorption spectra of the complex on a glass plate, both the $[Ru^{II}(OH)(Q)Ru^{II}(OH)(Q)]^{2+}/[Ru^{II}(OH)(SQ)Ru^{II}(OH)(SQ)]^0$ and $[Ru^{II}(O)(Q)Ru^{II}(O)(Q)]^{2+}/[Ru^{II}(O)(SQ)Ru^{II}(O)(SQ)]^0$ redox reactions (eqs 3 and 4) are expected to take place at +0.32 V. The irreversible anodic wave at +1.19 V is associated with two-electron oxidations of $[Ru^{II}(OH)(Q)Ru^{II}(OH)(Q)]^{2+}$ and $[Ru^{II}(O)(Q)Ru^{II}(O)(Q)]^{2+}$, affording $[Ru^{III}(OH)(Q)Ru^{III}(OH)(Q)]^{4+}$ and $[Ru^{III}(O)(Q)Ru^{III}(O)(Q)]^{4+}$, respectively. Strong anodic currents at potentials more positive than +1.2 V are apparently caused by the oxidation of water. The irreversible anodic currents observed at pH 4.0 decreased by about half at pH 3.0 and completely disappeared at pH 1.8. In harmony with this, an anodic wave due to catalytic oxidation of water was not observed in the CV of $[\mathbf{1}]^{2+}$ in the absence of water in CF_3CH_2OH/ether (Figure 5). These facts indicate that oxidation of water by the oxidized form of $[\mathbf{1}]^{2+}$ does not proceed unless the complex dissociates protons. Thus, $[Ru^{III}(O)(Q)Ru^{III}(O)(Q)]^{4+}$, not $[Ru^{III}(OH)(Q)Ru^{III}(OH)(Q)]^{4+}$, is considered to be the active form for water oxidation.

An ITO electrode slowly evolved O_2 even in the absence of $[\mathbf{1}]^{2+}$ under controlled-potential electrolysis at +1.70 V above pH 5.0. Such water oxidation by an ITO electrode was safely avoided when electrolysis was carried out in water at pHs lower than 4.0. The controlled-potential electrolysis of [**1**]$(SbF_6)_2$ modified on an ITO electrode, therefore, was conducted at

(22) The parent peak of $[\mathbf{1}]^{2+}$ ($m/z = 659$) disappeared in the ESI-MS spectra of the electrolysis solution after the catalytic currents had completely ceased.

+1.70 V (vs Ag/AgCl) in water (pH 4.0), and 1.5 mL of O_2 was generated after 27.5 C passed in the electrolysis. The current efficiency for O_2 evolution was 95% and the turnover number was 2400 based on the complex. The current density of the electrode was 0.12 mA/cm^2 in the initial stage. The current gradually decreased with decrement of pH in the aqueous phase and almost ceased at pH 1.2. The current density of the electrode for the oxidation of water was recovered when the pH of water was readjusted to 4.0 by the addition of aqueous KOH to the aqueous phase. The oxidation of water by [**1**](SbF$_6$)$_2$ modified on an ITO electrode finally evolved 15.2 mL of O_2 (turnover number: 33 500) in 40 h, and then the O_2 evolution completely ceased owing to gradual exfoliation of [**1**](SbF$_6$)$_2$ from the surface of the ITO electrode. Thus, [**1**](SbF$_6$)$_2$ modified on ITO catalyzed water oxidation with an excellent turnover number compared to the case of [**1**]$^{2+}$ in CF_3CH_2OH. Such a great difference in catalytic ability probably results from the high stability of [**1**]$^{2+}$ in the solid state compared with that in CF_3CH_2OH solution.

The CV of the ITO electrode modified with the bipyridine complex [**2**](SbF$_6$)$_2$ is also depicted in Figure 6b. Taking into account that the hydroxo ligands of [**2**](SbF$_6$)$_2$ did not dissociate protons under the experimental conditions, we assign the nearly reversible feature at $E_{1/2} = +0.79$ V to the [Ru^{II}(OH)(bpy)-Ru^{II}(OH)(bpy)]$^{2+}$/[Ru^{III}(OH)(bpy)Ru^{III}(OH)(bpy)]$^{4+}$ redox couple. Although the CV of [**2**](SbF$_6$)$_2$ modified on ITO showed catalytic currents due to the oxidation of water at potentials more positive than +1.5 V, the currents are much smaller than that of [**1**](SbF$_6$)$_2$ modified on ITO. In fact, anodic currents hardly flowed in the controlled-potential electrolysis of [**2**](SbF$_6$)$_2$ modified on ITO at +1.70 V in H_2O (pH 4.0) and the amount of O_2 evolved was too small to detect by GC.

Mechanisms of Water Oxidation Catalyzed by [1]$^{2+}$. In contrast to [**1**]$^{2+}$, which showed catalytic activity for the oxidation of water, the analogous monomeric complex [Ru(OH$_2$)(3,5-^{t}Bu$_2$qui)(terpy)](ClO$_4$)$_2$ showed no catalytic currents for the oxidation of water in H_2O under similar conditions. The two ruthenium−hydroxo units of [**1**]$^{2+}$, therefore, play the key role in the oxidation of water. A proposed mechanism for the water oxidation catalyzed by [**1**]$^{2+}$ modified on ITO in water is depicted in Scheme 3. Reduction of the quinones to semiquinones coupled with the dissociation of the hydroxo protons of [**1**]$^{2+}$ is attributable to the intramolecular electron transfer from the resultant oxo ligands to quinone ligands. Such electron transfer would induce radical character on the two oxo ligands of [Ru(O)(SQ)Ru(O)(SQ)]^0, which must be placed adjacently inside the cavity formed by the two bulky semiquinone ligands and by btpyan. As a result, the O−O bond is probably formed by the intramolecular coupling reaction between the two oxo ligands of [Ru(O)(SQ)Ru(O)(SQ)]^0. The resultant [Ru(O)(SQ)-Ru(O)(SQ)]^0 complex undergoes two types of successive oxidation reactions: the first is the ligand-localized oxidation of semiquinone to quinone at +0.4 V, producing [Ru(O)(Q)-Ru(O)(Q)]$^{2+}$, and the second is the metal-centered oxidation of Ru^{II} to Ru^{III} at +1.2 V, affording [Ru^{III}(O)(Q)Ru^{III}(O)(Q)]$^{4+}$. Dissociation of O_2 from [(Q)Ru^{II}−O═O−Ru(Q)]$^{4+}$ as the hybridization isomer of [Ru^{III}(O)(Q)Ru^{III}(O)(Q)]$^{4+}$ and the subsequent coordination of two H_2O ligands to the coordinatively unsaturated Ru^{II} center affords [Ru(OH$_2$)(Q)Ru(OH$_2$)-(Q)]$^{4+}$, which spontaneously dissociates aqua protons at pH 4 to regenerate [Ru(O)(SQ)Ru(O)(SQ)]^0. Thus, the pH of the aqueous phase is of fundamental importance to the O−O bond formation and the regeneration of [**1**]$^{2+}$ in the catalytic cycle (Scheme 3). In fact, the catalytic currents of the water oxidation by the [**1**](SbF$_6$)$_2$ modified on ITO at potentials more positive than +1.2 V at pH 4.0 decreased to half at pH 3 and were not detected at pH 1.2. It is worthy of note that the pathway for the formation of [Ru(O)(Q)Ru(O)(Q)]$^{2+}$ in CF_3CH_2OH/H_2O is different from Scheme 3 because [**1**]$^{2+}$ does not dissociate two protons in CF_3CH_2OH/H_2O. [**1**]$^{2+}$ is oxidized at +1.34 V to produce [Ru(O)(Q)Ru(O)(Q)]$^{2+}$ with the dissociation of two protons. Thus, [**1**]$^{2+}$ dissociates two protons in H_2O at pH >4 prior to the oxidation, while two protons are liberated from the two-electron oxidation product of [**1**]$^{2+}$ in CF_3CH_2OH.

Scheme 3. Proposed Mechanism for Water Oxidation Catalyzed by [**1**](SbF$_6$)$_2$ Modified on an ITO Electrode in Water

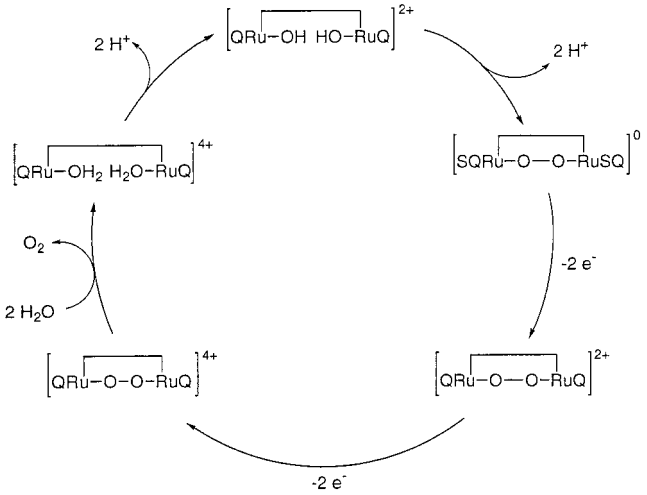

The distinct difference in the catalytic abilities of [**1**]$^{2+}$ and [**2**]$^{2+}$ for water oxidation is reasonably associated with the function of the quinones in the former. Ligand-localized oxidation of [Ru^{II}(O)(SQ)Ru^{II}(O)(SQ)]^0 formed by dissociation of protons from [Ru^{II}(OH)(Q)Ru^{II}(OH)(Q)]$^{2+}$ (eq 2) involves two of the four electrons in the water oxidation, and metal-centered oxidation of the resultant [Ru^{II}(O)(Q)Ru^{II}(O)(Q)]$^{2+}$ complex accounts for the remaining two electrons in the four-electron oxidation of water. Four-electron oxidation of water is achieved by redox reactions of not only the two Ru(II)/Ru(III) couples but also the two semiquinone/quinone couples, while [**2**]$^{2+}$ has only the two Ru sites.

Acknowledgment. This work was partly supported by a Grant-in-Aid for Scientific Research on Priority Areas from the Ministry of Education, Science, Sports, and Culture of Japan (No. 10149259).

Supporting Information Available: A printout of the CIF file for the X-ray structure determination of 1,8-bis(2,2′:6′,2″-terpyridyl)-anthracene and a figure showing electronic absorption spectra of [**1**]$^{2+}$ modified on a glass plate in water. This material is available free of charge via the Internet at http://pubs.acs.org.

IC000552I